frontiers | Frontiers in Physiology

TYPE Original Research
PUBLISHED 15 October 2024
DOI 10.3389/fphys.2024.1435594



OPEN ACCESS

EDITED BY
James Cray,
The Ohio State University, United States

REVIEWED BY
Noriaki Ono,
University of Texas Health Science Center at Houston, United States
Hiroyuki Yamaguchi,
University of Texas Health Science Center at Houston, United States

*CORRESPONDENCE
Erin Ealba Bumann,
bumanne@umkc.edu

†PRESENT ADDRESS
Erin Ealba Bumann,
Department of Oral and Craniofacial Sciences, University of Missouri-Kansas City School of Dentistry, Kansas City, MO, United States

RECEIVED 20 May 2024
ACCEPTED 19 June 2024
PUBLISHED 15 October 2024

CITATION
Houchen CJ, Ghanem S, Kaartinen V and Bumann EE (2024), TGF-β signaling in the cranial neural crest affects late-stage mandibular bone resorption and length. *Front. Physiol.* 15:1435594. doi: 10.3389/fphys.2024.1435594



# TGF-β signaling in the cranial neural crest affects late-stage mandibular bone resorption and length

Claire J. Houchen[1], Saif Ghanem[2], Vesa Kaartinen[2] and Erin Ealba Bumann[1,3]*†

[1]Department of Oral and Craniofacial Sciences, University of Missouri-Kansas City School of Dentistry, Kansas City, MO, United States, [2]Department Biologic and Materials Sciences, University of Michigan School of Dentistry, Ann Arbor, MI, United States, [3]Department of Orthodontics and Pediatric Dentistry, University of Michigan School of Dentistry, Ann Arbor, MI, United States

Malocclusions are common craniofacial malformations that cause quality of life and health problems if left untreated. Unfortunately, the current treatment for severe skeletal malocclusion is invasive surgery. Developing improved therapeutic options requires a deeper understanding of the cellular mechanisms responsible for determining jaw bone length. We have recently shown that neural crest mesenchyme (NCM) can alter jaw length by controlling the recruitment and function of mesoderm-derived osteoclasts. Transforming growth factor beta (TGF-β) signaling is critical to craniofacial development by directing bone resorption and formation, and heterozygous mutations in the TGF-β type I receptor (*TGFBR1*) are associated with micrognathia in humans. To identify the role of TGF-β signaling in NCM in controlling osteoclasts during mandibular development, the mandibles of mouse embryos deficient in the gene encoding *Tgfbr1*, specifically in NCM, were analyzed. Our laboratory and others have demonstrated that *Tgfbr1*$^{fl/fl}$*;Wnt1-Cre* mice display significantly shorter mandibles with no condylar, coronoid, or angular processes. We hypothesize that TGF-β signaling in NCM can also direct late bone remodeling and further regulate late embryonic jaw bone length. Interestingly, analysis of mandibular bone based on micro-computed tomography and Masson's trichrome revealed no significant difference in bone quality between the *Tgfbr1*$^{fl/fl}$*;Wnt1-Cre* mice and controls, as measured by the bone perimeter/bone area, trabecular rod-like diameter, number and separation, and gene expression of collagen type 1 alpha 1 (*Col1α1*) and matrix metalloproteinase 13 (*Mmp13*). Although there was not a difference in localization of bone resorption within the mandible indicated by tartrate-resistant acid phosphatase (TRAP) staining, *Tgfbr1*$^{fl/fl}$*;Wnt1-Cre* mice had approximately three-fold less osteoclast number and perimeter than controls. Gene expression of receptor activator of nuclear factor kappa-β (*Rank*) and *Mmp9*, markers of osteoclasts and their activity, also showed a three-fold decrease in *Tgfbr1*$^{fl/fl}$*;Wnt1-Cre* mandibles. Evaluation of osteoblast-to-osteoclast signaling revealed no significant difference between *Tgfbr1*$^{fl/fl}$*;Wnt1-Cre* mandibles and controls, leaving the specific mechanism unresolved. Finally, pharmacological inhibition of *Tgfbr1* signaling during the initiation of bone mineralization and resorption significantly shortened jaw length in embryos. We conclude that TGF-β signaling in NCM decreases mesoderm-derived

osteoclast number, that TGF-β signaling in NCM impacts jaw length late in development, and that this osteoblast-to-osteoclast communication may be occurring through an undescribed mechanism.

KEYWORDS

**transforming growth factor beta type I receptor, jaw, mandible, neural crest, bone resorption, osteoclasts, bone remodeling, maxillofacial development**

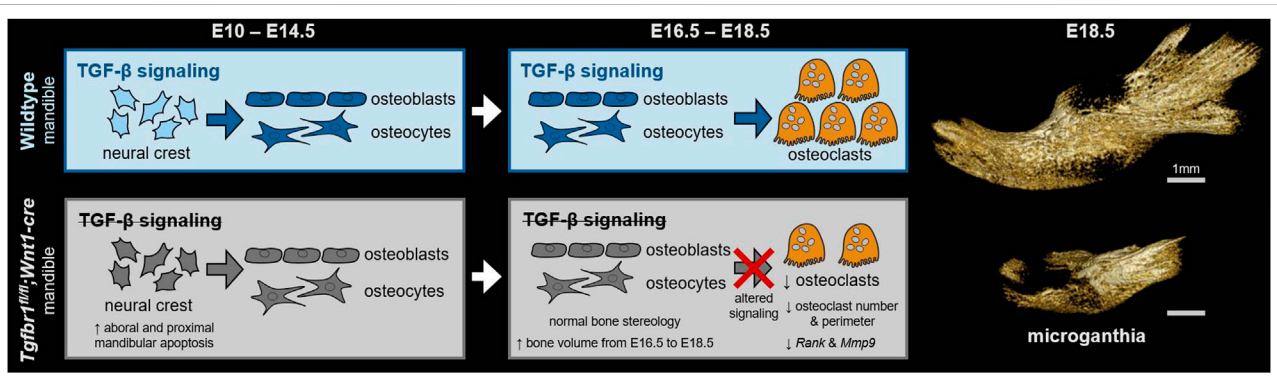


GRAPHICAL ABSTRACT

# 1 Introduction

Craniofacial anomalies are a diverse group of malformations in the growth of the skull and facial bones. These anomalies can be inherited or spontaneous, and both genetic and environmental factors have important influences on craniofacial development (Cakan et al., 2012). Craniofacial anomalies present a significant clinical issue because the only treatment option currently available is invasive surgery (Gorlin et al., 1990; Albanese and Harrison, 1998). The jaw skeleton, specifically, displays a wide range of anomalies, including hypo- and hyperplasia, pro- and retrognathia, and micro- and macroganthia. Increasing our understanding of the molecular and cellular mechanisms by which elements of the jaw skeleton achieve their appropriate shape and size also increases our ability to develop minimally invasive therapeutic options to improve the quality of life for patients with jaw anomalies.

During embryonic development, neural crest mesenchyme (NCM) forms all the bony elements in the facial and jaw skeletons. NCM-derived osteoblast lineage cells form the bone and NCM-derived chondrocyte lineage cells form the cartilage of the facial and jaw bones (Hall et al., 2014). NCM is known to specifically be involved in osteogenic induction, proliferation, differentiation, mineralization, and matrix remodeling (Ealba et al., 2015; Prasad et al., 2019; Malik et al., 2020; Roth et al., 2021). It is well-established that osteoblast lineage cells such as osteocytes influence osteoclastogenesis and osteoclast function, and there is growing evidence that bone resorption by osteoclasts is critical to mandibular development (Tatsumi et al., 2007; Nakashima et al., 2011; Xiong et al., 2015). It is therefore logical that in addition to its long-known role in facial and jaw osteogenesis, NCM also regulates jaw length by controlling bone resorption, which has been demonstrated in both mice and birds (Ealba et al., 2015; Hassan et al., 2023; Houchen et al., 2023). The primary cell type known to play a role in bone resorption is mesoderm-derived osteoclasts, not an NCM-derived cell. An understanding of embryonic cellular signaling, particularly between NCM-derived osteoblast lineage cells and mesoderm-derived osteoclasts, is critical for understanding the origin of jaw bone anomalies in human patients.

One pathway that may be involved in communication between NCM-derived osteoblast lineage cells and mesoderm-derived osteoclasts is TGF-β signaling. The TGF-β signaling pathway is comprised of a heteromeric complex of two type one and two type two transmembrane serine/threonine kinases, TGFBR1 and TGFBR2 (Attisano and Wrana, 2002). Upon ligand binding, the activated TGF-β receptor complex phosphorylates Smad proteins that form a signal cascade that accumulates in the nucleus, where they serve as transcription factors (Massague and Wotton, 2000; Derynck and Zhang, 2003). The TGF-β signaling family is known to play an important role in embryonic craniofacial development, cell proliferation, migration and differentiation, and extracellular matrix secretion (Barlow and Francis-West, 1997; Oka et al., 2007; Zhao et al., 2008; Tang et al., 2012; Peters et al., 2017; Yuan et al., 2020). Within bone tissue, TGF-β is known to regulate many aspects of bone remodeling, such as osteoblast proliferation, osteoblast differentiation, and osteoclast apoptosis, through the modulation of factors such as matrix metalloproteinase 13 (Mmp13) (Alliston et al., 2001; Tang et al., 2012). Consequently, patients who are heterozygous for mutations in *TGFBR1* have Loeys–Dietz syndrome I, which is associated with craniofacial changes such as craniosynostosis, facial asymmetry, low-set ears, hypertelorism, a cleft palate, and microretrognathia (Lacombe and Battin, 1993; Loeys et al., 2005;

MacCarrick et al., 2014). Therefore, TGF-β signaling in NCM is critical during facial and jaw development, but it is not yet fully understood.

Previous studies have begun to explore TGF-β signaling in NCM and jaw development, and specifically, both TGFBR1 and TGFBR2 have emerged as regulators of mandible patterning (Oka et al., 2007; Peters et al., 2017; Yuan et al., 2020). Loss of *Tgfbr1* in NCM results in a shortened mandible and a lack of development of the coronoid, condylar, and angular processes (Dudas et al., 2006; Zhao et al., 2008). Previously, the mandibular defect in mice lacking *Tgfbr1* in NCM was attributed to high rates of apoptosis from stage E10 to E14.5 in the proximal and aboral regions of the mandible, while no changes in cell proliferation were noted (Dudas et al., 2006; Zhao et al., 2008). In this study, we elucidate the mechanism of NCM control of jaw development by modulating TGF-β signaling in NCM and investigating resulting bone resorption changes in the lower jaw. We hypothesized that in addition to high rates of apoptosis in the jaws of mice that lack *Tgfbr1* in NCM, osteoclastogenesis and bone resorption would be altered in the mandible due to the loss of typical TGF-β signaling in NCM-derived osteoblasts and osteocytes.

# 2 Materials and methods

## 2.1 Generation and genotyping of *Tgfbr1$^{fl/fl}$;Wnt1-Cre* mice

*Alk5$^{fl/fl}$* female mice (Larsson et al., 2001) were mated with *Wnt1-Cre* male mice (Danielian et al., 1998) to generate the *Alk5$^{fl/+}$/Wnt1-Cre* mice, and then the *Alk5$^{fl/fl}$* female mice were mated with *Alk5$^{fl/+}$/Wnt1-Cre* male mice to generate the experimental *Tgfbr1$^{fl/fl}$;Wnt1-Cre* embryos (Dudas et al., 2006; Zhao et al., 2008). *Tgfbr$^{fl/+}$* mice were used as experimental controls. All mice used in these studies are on a mixed C57BL6/J 129Sv background.

Genotyping was conducted using a MultiGene™ Gradient PCR Thermal Cycler (Labnet, Edison, NJ) or a Veriti™ 96-Well Fast Thermal Cycler (Thermo Fisher Scientific, Wilmington, DE) on tail tip and yolk sac DNA. Mutant embryos were identified by PCR genotyping for the presence of the *cre* transgene (forward 5′-CGT TTTCTGAGCATACCTGGA-3′ and reverse 5′-ATTCTCCCACCG TCAGTAGG-3′) and the *Tgfbr1* floxed alleles (forward 5′-GAG TCTGAAGCTTTGCAAG-3′ and reverse 5′-ATTAGCTAAGCC CCTTC-3′).

For staging, noon on the plugging day was designated as E0.5. Embryos were staged by comparison with references (Kaufman, 1992). Mouse embryos were collected for analysis at stages E16.5 and E18.5. Dams were euthanized by carbon dioxide followed by pneumothorax and the embryonic mice were euthanized by decapitation. All protocols were approved by the Institutional Animal Care and Use Committee at the University of Michigan (PRO00008469).

## 2.2 Microcomputed tomography analysis of mandibular bone

Specimens were placed in a 19-mm-diameter specimen holder and scanned over the entire skull using a microcomputed tomography (micro-CT) system (μCT 100 Scanco Medical, Bassersdorf, Switzerland). The following scan settings were used: 10 μm voxel size, 55 kVp, 109 μA, 0.5 mm AL filter, and 500 ms integration time. An analysis of bone volume and tissue mineral density was performed using manufacturer's evaluation software. A fixed global threshold of 13% (130 on a grayscale of 0–1000) for E16.5 mice and 15% (150 on a grayscale of 0–1000) for E18.5 mice was used to segment bone from non-bone. Four control and four *Tgfbr1$^{fl/fl}$;Wnt1-Cre* samples were assessed at both E16.5 and E18.5 (n = 4/genotype/stage).

## 2.3 Whole-mount staining of tartrate-resistant acid phosphatase

To detect bone resorption, embryos were fixed in 10% formalin overnight at 4°C and stained to identify tartrate-resistant acid phosphatase (TRAP) activity. Samples were stained whole-mount using an Acid Phosphatase Leukocyte Kit, following the manufacturer's protocol, except Fast Red Violet was used in place of Fast Garnet GBC Base Solution (Sigma-Aldrich, Saint Louis, MO) (Ealba et al., 2015). Seventeen control and nine *Tgfbr1$^{fl/fl}$;Wnt1-Cre* samples were assessed from four litters. Images of the embryos were taken on an MZ95 Microscope (Leica, Buffalo Grove, IL) with a DP72 camera using cellSens Entry software (Olympus, Center Valley, PA).

## 2.4 Histology

To examine bone quality and bone resorption on the cellular level, embryos were fixed in 10% formalin overnight at 4°C, washed in PBS, decalcified in EDTA/Tris-buffered saline for 1–3 days at 4°C, dehydrated, embedded in paraffin, and cut into 7 μm transverse sections. To analyze mandibular bone quality, sections were stained with Masson's trichrome: Bouin's fluid overnight, Mayer's hematoxylin for 10 min, Biebrich scarlet for 2 min, phosphomolybdic acid/phosphotungstic acid for 15 min, and aniline blue for 15 min. To identify bone resorption in the mandible, adjacent sections to each Masson's trichrome were stained with TRAP as described above for the whole-mount embryos and counterstained with fast green (Vector Laboratories, Burlingame, CA).

Images were obtained on a BX51 Upright Light Microscope with a DP70 camera using DP Controller software (Olympus) or an Axiovert 200M Microscope with an AxioCam MRx using AxioVision 4.8 software (Zeiss, Thornwood, NY). For the images collected using DP controller software, Image Composite Editor software (Microsoft Research, Redmond, WA) was used to stitch multiple images into one.

Bioquant Osteo 2014 v141.60 software (Bioquant Image Analysis Corporation, Nashville, TN) was used to quantify mandibular bone quality using Masson's trichrome-stained sections and mandibular bone resorption using TRAP/fast green-stained sections. Bone quality was assessed by the following measures: bone perimeter per bone area (B.Pm/B.Ar), trabecular rod-like width (Tb.W), trabecular number (Tb.N), and trabecular

10.3389/fphys.2024.1435594

TABLE 1 TaqMan primers. TaqMan primers for *Mmp13*, *Mmp9*, *Rankl*, *Opg*, *Rank*, and *M-csf* are listed along with their amplicon lengths.

| Gene | TaqMan assay | Amplicon length |
|---|---|---|
| *Mmp13* | Mm00439491_m1 | 65 |
| *Mmp9* | Mm00442991_m1 | 76 |
| *Rankl* | Mm00441906_m1 | 66 |
| *Opg* | Mm01205928_m1 | 75 |
| *Rank* | Mm00437132_m1 | 65 |
| *M-csf* | Mm00432686_m1 | 70 |

separation (Tb.Sp). Bone resorption was assessed by osteoclast perimeter per bone area (Oc.Pm/B.Ar) and number of osteoclasts per bone area (Oc.N/B.Ar) in sections adjacent to sections used for bone quality analysis (Dempster et al., 2013). Three control and three *Tgfbr1*$^{fl/fl}$*;Wnt1-Cre* E18.5 embryos from the same litter were assessed.

## 2.5 Gene expression analysis by RT-qPCR

Expression of genes related to osteoblasts, osteoclasts, and osteoblast-to-osteoclast signaling was assessed by reverse transcription quantitative PCR (RT-qPCR) (Bustin et al., 2009). Total RNA was isolated from E18.5 mandibles with the soft tissue removed using an RNeasy Column Purification Kit (QIAGEN, Valencia, CA). The ascending ramus was removed from control samples because *Tgfbr1*$^{fl/fl}$*;Wnt1-Cre* lacked the ascending ramus and all mandibular processes (Atchley and Hall, 1991; Atchley, 1993; Ehrich et al., 2003; Klingenberg et al., 2003). The concentration and purity of RNA were assessed using a NanoDrop ND-1000 Spectrophotometer (Thermo Fisher Scientific). Approximately 560 ng of total RNA was converted to cDNA in a 20 µL reverse transcription reaction using the Omniscript RT Kit (QIAGEN) and random primers (Thermo Fisher Scientific). The reaction was processed for 90 min at 37°C and then stored at −20°C.

RT-qPCR was performed in a ViiA™ 7 Real-Time PCR System (Thermo Fisher Scientific, Grand Island, NY). Forward and reverse primers, 1 µL of cDNA, RNase-free dH20, and TaqMan Universal PCR Master Mix (Thermo Fisher Scientific), containing dNTPs with dUTP, AmpliTaq Gold DNA polymerase, Uracil-DNA Glycosylase, Passive Reference 1, and optimized buffer components, were manually mixed in a 30 µL reaction to amplify the cDNA of interest. Samples were run on MicroAmp Optical 96-well Reaction Plates (Thermo Fisher Scientific). The thermal cycling parameters for all primers were as follows: step 1, 50°C for 2 min; step 2, 95°C for 10 min; step 3, 60°C for 1 min and a plate read; step 3 was repeated 40 times; and step 4, 60°C for 1 min. PCR products amplified after 35 cycles were considered to be false positives. Roche Applied Science ProbeFinder was used to design the following mouse gene primers: *β-actin* (forward 5′–TGACAGGATGCA GAAGGAGA–3′ and reverse 5′–CGCTCAGGAGGAGCA ATG–3′), used with Universal primer #106 with an amplicon length of 75 bp and collagen type 1 alpha 1 (*Col1α1*) (forward 5′–CATGTTCAGCTTTGTGGACCT–3′ and reverse 5′–GCAGCT GACTTCAGGGATGT–3′), used with Universal primer #15, with an amplicon length of 94 bp. Primers for mouse *Mmp13, Mmp9, Rank, Rankl, Opg*, and *M-csf* are commercially available from Thermo Fisher Scientific (see Table 1 for primer sequences).

Expression of *Col1α1, Mmp13, Mmp9, Rankl, Opg, Rank*, and *M-csf* were normalized to the expression of the reference gene *β-actin*. Amplification efficiencies were monitored across samples to ensure they remained sufficiently equal. Fold changes were calculated using the delta–delta C(t) method (Livak and Schmittgen, 2001). To assess relative fold changes between genotypes, *Tgfbr1*$^{fl/fl}$*;Wnt1-Cre* mice were compared relative to control mice at E18.5. Four control and four *Tgfbr1*$^{fl/fl}$*;Wnt1-Cre* embryos from the same litter were assessed.

## 2.6 Use of quail embryos

Fertilized eggs of Japanese quail (*Coturnix japonica*) were acquired from the Michigan State University Poultry Farm (Lansing, MI) and incubated at 37°C in a humidified chamber until they reached embryonic stages appropriate for injections and analyses. The Hamburger–Hamilton (HH) staging system was used to properly stage quail embryos (Hamburger and Hamilton, 1951; Ainsworth et al., 2010). For all procedures, we adhered to accepted practices for the humane treatment of avian embryos as described in S3.4.4 of the *AVMA Guidelines for the Euthanasia of Animals*; 2013 Edition (Leary et al., 2022).

## 2.7 Inhibition of TGFBR1 in quail embryos

Quail eggs were windowed at HH9.5 using surgical scissors and transparent tape. Ten microliters of the TGFBR1 inhibitor (iTGFBR1) SB431542 (Sigma, SB) was injected into the vitelline vein of quail at stage HH33, which by Carnegie staging is similar to an E15 mouse, and therefore, after the E10–E14.5 apoptosis phenotype seen in the *Tgfbr1*$^{fl/fl}$*;Wnt1-Cre* mouse embryos (Hamburger and Hamilton, 1951; Theiler, 2013). The concentration was determined following dose-response studies and published literature. Control embryos were treated with vehicle dimethylsulfoxide (DMSO). After injections, eggs were closed with tape and incubated until they were collected in 10% formalin at stage HH38. Five control vehicle-injected quail and four iTGFBR1-injected quail were assessed. All samples were injected and collected at the same time.

## 2.8 Whole-mount staining of calcified bone using alizarin red

To analyze the skull and lower jaw bone morphology of control and iTGFBR1-treated quail embryos, HH38 embryos were collected in water, eviscerated, and fixed in 95% ethanol. Acetone was used to remove the fat tissue. Five control and four iTGFBR1-treated quail embryos were then stained with alizarin red to identify calcified bone. Tissue was cleared in 0.5% KOH and 0.06% $H_2O_2$ and then processed through a glycerol series (25%, 50%, 75%, and 100%)

(Nagy, 2003; Dudas et al., 2006; Zhao et al., 2008; Hall et al., 2014; Ealba et al., 2015).

Alizarin red-stained control and iTGFBR1-treated quail embryos were imaged on an MZ95 Microscope (Leica, Buffalo Grove, IL) with a DP72 camera using cellSens Entry software (Olympus, Center Valley, PA).

## 2.9 Measurement of jaw length in quail embryos

Lower jaw length of n = 5 control and n = 4 iTGFBR1-treated quail embryos was quantified using ImageJ (Schneider et al., 2012). Lower jaw length was assessed using lateral micrographs by measuring from the proximal tip of the angular bone to the distal tip of the dentary bone. Upper jaw length was assessed using the same lateral micrographs by measuring from the tip of the nasal bone in the center of the maxilla to the distal tip of the premaxilla. Proportional lower jaw length is depicted as a lower jaw to upper jaw ratio to normalize for skull size.

## 2.10 Statistics

Bone stereology and osteoclast measures assessed with BioQuant Osteo data are represented as the median ± interquartile range, with all points shown and compared using the Wilcoxon rank sum test. Bone volume and tissue mineral density measures from micro-CT scans show the mean relative to controls ±standard deviation. Gene expression data are represented as the mean fold change ±standard deviation, with all data points shown. Quail jaw proportion data are represented as the median ± interquartile range with all points shown. Micro-CT, gene expression, and quail jaw proportion data were assessed using an unpaired Student's t-test.

# 3 Results

*Tgfbr1*$^{fl/fl}$*;Wnt1-Cre* embryos at E18.5 had a severe micrognathia phenotype and lacked all condylar, coronoid, and angular processes consistent with the phenotype of these mice previously described by Dudas et al., 2006 and Zhao et al., 2008 (Figures 1A, B). In addition to the mandibular changes in *Tgfbr1*$^{fl/fl}$*;Wnt1-Cre* embryos, the craniofacial defects of *Tgfbr1*$^{fl/fl}$*;Wnt1-Cre* embryos were severe and led to perinatal lethality (data not shown (Dudas et al., 2006; Zhao et al., 2008)). Masson's trichrome staining of control *Tgfbr1*$^{fl/+}$ and *Tgfbr1*$^{fl/fl}$*;Wnt1-Cre* mandibles showed dramatic gross changes in mandibular anatomy at the molar, incisor, and ventral levels of *Tgfbr1*$^{fl/fl}$*;Wnt1-Cre* embryos (Figures 1C, D). Surprisingly, closer histological analysis of the blue-stained mandibular bone did not reveal a stark difference in bone architecture between control and *Tgfbr1*$^{fl/fl}$*;Wnt1-Cre* E18.5 embryos (Figures 1E, F). Furthermore, bone quality and stereology analysis revealed that *Tgfbr1*$^{fl/fl}$*;Wnt1-Cre* embryos did not differ from control embryos in bone perimeter per bone area, trabecular-like width, trabecular-like number, or trabecular-like separation, which further suggests bone quality did not significantly differ between control and *Tgfbr1*$^{fl/fl}$*;Wnt1-Cre* E18.5 embryos (Figures 1G-J). Additionally, expression of *Col1α1* and *Mmp13*, and markers of bone deposition and activity, did not differ in the mandible between the control and *Tgfbr1*$^{fl/fl}$*;Wnt1-Cre* E18.5 embryos (Figures 1K, L). These data suggest minimal changes in mandibular bone quality in *Tgfbr1*$^{fl/fl}$*;Wnt1-Cre* mandibles despite severe micrognathia and perinatal lethal craniofacial defects.

To evaluate mandibular development between E16.5 and E18.5, embryonic control and *Tgfbr1*$^{fl/fl}$*;Wnt1-Cre* mandibles were imaged by micro-CT to visualize the ossified bone at each of these stages (Figures 2A–H). To evaluate mandibular bone resorption between E16.5 and E18.5, embryonic control and *Tgfbr1*$^{fl/fl}$*;Wnt1-Cre* mandibles were stained for TRAP, which visualizes bone resorption in red (Figures 2I–P). At both E16.5 and E18.5, the macroscopic spatial pattern of mandibular bone resorption did not greatly differ between embryonic control and *Tgfbr1*$^{fl/fl}$*;Wnt1-Cre* mandibles despite drastic morphological differences in the mandible between the two genotypes. Bone stereology could not be compared between E16.5 and E18.5 because the E16.5 embryos lacked sufficient bone tissue for quantitative analysis. In addition to morphological differences in *Tgfbr1*$^{fl/fl}$*;Wnt1-Cre* mandibles, bone volume was significantly decreased in *Tgfbr1*$^{fl/fl}$*;Wnt1-Cre* mandibles at E16.5 and E18.5; *Tgfbr1*$^{fl/fl}$*;Wnt1-Cre* mandibles had 86% less bone volume relative to controls at E16.5 (Figure 2Q) and 72% less bone volume relative to controls at E18.5 (Figure 2R). While bone volume was significantly lower in *Tgfbr1*$^{fl/fl}$*;Wnt1-Cre* mandibles at both E16.5 and E18.5, *Tgfbr1*$^{fl/fl}$*;Wnt1-Cre* mandible bone volume increased approximately two times more than control mandible bone volume between these two stages. Although bone volume differed significantly between genotypes, tissue mineral density did not differ significantly between groups (Figures 2S, T), which mirrors the lack of bone stereology differences between *Tgfbr1*$^{fl/fl}$*;Wnt1-Cre* and control mandibles as well as the retained pattern of bone resorption in *Tgfbr1*$^{fl/fl}$*;Wnt1-Cre* mandibles.

TRAP-stained sections at the molar, incisor, and ventral levels of the mandible (Figures 3A–D) revealed on the microscopic level that the conditional knock out of *Tgfbr1* in NCM-derived osteoblasts resulted in a significant 3.2-fold decrease in osteoclast number per bone area in *Tgfbr1*$^{fl/fl}$*;Wnt1-Cre* mandibles (Figure 3E). Additionally, osteoclast perimeter per bone area significantly decreased by 3.2-fold in *Tgfbr1*$^{fl/fl}$*;Wnt1-Cre* mandibles compared to controls (Figure 3F). These data show that there are fewer osteoclasts within the same bone area in the *Tgfbr1*$^{fl/fl}$*;Wnt1-Cre* mandibles. Receptor activator of nuclear factor kappa-B (*Rank*) expression decreased 2.5-fold in *Tgfbr1*$^{fl/fl}$*;Wnt1-Cre* mandibles, similarly suggesting a decrease in osteoclasts (Figure 3G). However, matrix metalloproteinase 9 (*Mmp9*) expression decreased only 0.64-fold in *Tgfbr1*$^{fl/fl}$*;Wnt1-Cre* mandibles, demonstrating a non-significant decrease in active bone resorption (Figure 3H).

As osteoclasts are mesoderm-derived, not NCM-derived or targeted directly by Wnt1-Cre, they should retain *Tgfbr1*. Consequently, changes in osteoclasts in *Tgfbr1*$^{fl/fl}$*;Wnt1-Cre* mandibles must be due to alterations in another cell type. Genes known to directly influence osteoclastogenesis were analyzed to investigate the possibility that changes in mesoderm-derived osteoclasts in *Tgfbr1*$^{fl/fl}$*;Wnt1-Cre* mandibles were due to altered signaling from NCM-derived osteoblast lineage cells ("osteoblast-to-osteoclast signaling"). Expression of osteoblast- and osteocyte-secreted Rank ligand (*Rankl*) and *Rankl*'s inhibitor osteoprotegerin (*Opg*) did not differ significantly between *Tgfbr1*$^{fl/fl}$*;Wnt1-Cre* and control mandibles (Figures 4A, B). As

10.3389/fphys.2024.1435594

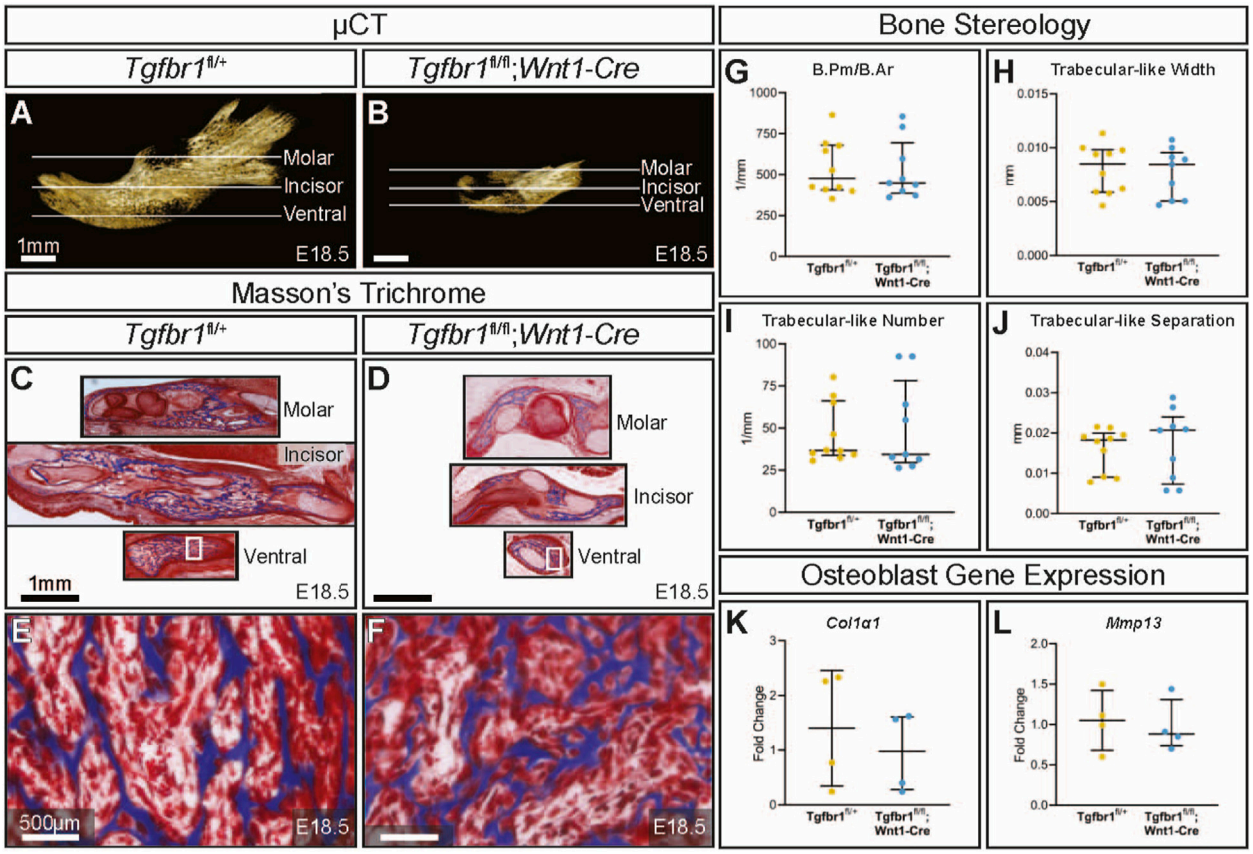


FIGURE 1
TGF-β signaling in the neural crest does not affect mandibular bone quality. Lateral views of micro-CT-scanned E18.5 **(A)** control and **(B)** *Tgfbr1*$^{fl/fl}$;*Wnt1-Cre* mouse mandibles show differences in overall size and shape. Transverse sections were analyzed from three different regions in the mandible: molar, incisor, and ventral. Sections from the mandibles were stained with Masson's trichrome, which stains bone blue, from **(C)** control and **(D)** *Tgfbr1*$^{fl/fl}$;*Wnt1-Cre* littermate E18.5 embryos. Higher magnification images from Masson's trichrome-stained ventral sections (white boxes) are shown for **(E)** control and **(F)** *Tgfbr1*$^{fl/fl}$;*Wnt1-Cre* littermate E18.5 embryos. The sections were analyzed to determine whether there were differences in bone stereology. There were no significant differences in **(G)** bone perimeter (B.Pm) per bone area (B.Ar), **(H)** trabecular-like width, **(I)** trabecular-like number, and **(J)** trabecular-like separation between the controls (blue) and *Tgfbr1*$^{fl/fl}$;*Wnt1-Cre* mice (cKO, yellow). Using RT-qPCR to assay for **(K)** *Col1α1* and **(L)** *Mmp13* mRNA as markers for bone deposition shows no significant difference in *Tgfbr1*$^{fl/fl}$;*Wnt1-Cre* (yellow) at E18.5 compared to controls (blue).

*Opg* inhibits *Rankl*, the *Rankl* to *Opg* ratio was also analyzed. Although the *Rankl* to *Opg* ratio trended downward in *Tgfbr1*$^{fl/fl}$;*Wnt1-Cre* mandibles, the difference between *Tgfbr1*$^{fl/fl}$;*Wnt1-Cre* and control mandibles was not significantly different (Figure 4C). Macrophage colony-stimulating factor (*M-csf*) similarly trended downward in *Tgfbr1*$^{fl/fl}$;*Wnt1-Cre* mandibles, but the decrease in *M-csf* expression in *Tgfbr1*$^{fl/fl}$;*Wnt1-Cre* mandibles was not statistically significant (Figure 4D). Therefore, while the severely micrognathic *Tgfbr1*$^{fl/fl}$;*Wnt1-Cre* mandibles had decreased osteoclast number per bone area, osteoclast perimeter per bone area, and *Rank* expression despite mesoderm-derived osteoclasts retaining *Tgfbr1*, the mechanism is not due to drastic changes in *Rankl*, *Opg*, *Rankl* to *Opg* ratio, or *M-csf* expression.

To further interrogate the role of TGF-β signaling at a more specific developmental timepoint, a single dose of an inhibitor of TGFBR1 (iTGFBR1) or vehicle control was delivered to embryonic quail at the developmental timepoint HH33, which by Carnegie staging is similar to an E15 mouse. This timepoint is critical, occurring after the E10–E14.5 apoptosis phenotype seen in *Tgfbr1*$^{fl/fl}$;*Wnt1-Cre* mouse embryos and just prior to osteoclast bone resorption begins in the lower jaw. Several days after iTGFBR1 or vehicle treatment at developmental stage HH38, when the jaw is ossified, vehicle control-treated quail embryos stained with alizarin red demonstrate typical quail jaw morphology, with the distal tip of the lower jaw being aligned with the upper jaw (Figure 4E). In contrast, iTGFBR1-treated quail embryos have a shorter lower jaw compared to the upper jaw (Figure 4F). To account for potential changes in upper jaw length, jaw length was assessed as lower-to-upper jaw ratio. Quail embryos given a single treatment of iTGFBR1 showed a significant 6.3% decrease in the lower-to-upper jaw ratio (Figure 4G). The decrease in lower jaw length observed in iTGFBR1-treated quail embryos recapitulates the micrognathia observed in *Tgfbr1*-deficient *Tgfbr1*$^{fl/fl}$;*Wnt1-Cre* mouse embryos.

## 4 Discussion

It has previously been established in separate reports 1) that NCM-derived osteoblast lineage cells influence embryonic mandibular development by controlling osteoclastogenesis and bone resorption

10.3389/fphys.2024.1435594

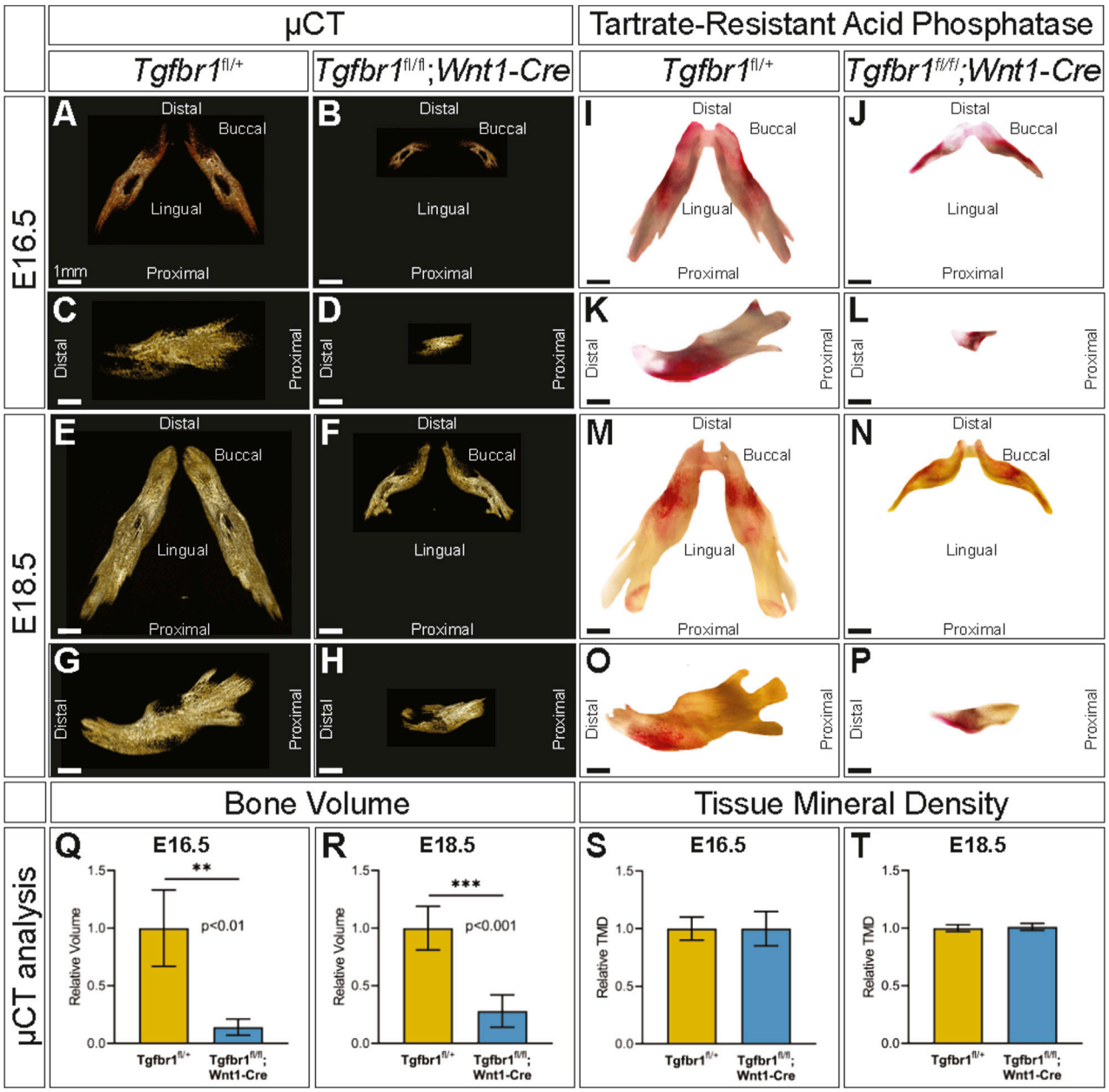


FIGURE 2
TGF-β signaling in the neural crest does not control the spatial pattern of mandibular bone resorption or tissue mineral density. Micro-CT-scanned mandibles from control and *Tgfbr1*$^{fl/fl}$;*Wnt1-Cre* E16.5 littermate embryos: **(A,B)** dorsal and **(C,D)** lateral views. E18.5 littermate embryos: **(E,F)** dorsal and **(G,H)** lateral views. TRAP-stained mandibles from control and *Tgfbr1*$^{fl/fl}$;*Wnt1-Cre* E16.5 littermate embryos: **(I,J)** dorsal and **(K,L)** lateral views and E18.5 littermate embryos: **(M,N)** dorsal and **(O,P)** lateral views. Micro-CT analysis of bone volume from **(Q)** E16.5 and **(R)** E18.5 control and *Tgfbr1*$^{fl/fl}$;*Wnt1-Cre* embryos and tissue mineral density from **(S)** E16.5 and **(T)** E18.5 control and *Tgfbr1*$^{fl/fl}$;*Wnt1-Cre* embryos.

and 2) that loss of TGFBR1 in NCM results in micrognathic jaws that lack the coronoid, condylar, and angular processes (Dudas et al., 2006; Zhao et al., 2008; Ealba et al., 2015). In this study, we investigated the possibility that TGF-β signaling in NCM is a critical signaling pathway through which NCM-derived osteoblast lineage cells influence osteoclast recruitment and osteoclast activity during mandibular development. Despite drastic craniofacial and mandibular defects, *Tgfbr1*$^{fl/fl}$;*Wnt1-Cre* mice, which lacked the Tgfbr1 receptor in NCM, had mandibular bone quality similar to controls, mandibular tissue mineral density similar to controls, and mandibular bone resorption, which was macroscopically similarly located to bone resorption in control mandibles. However, closer histological investigation revealed that *Tgfbr1*$^{fl/fl}$;*Wnt1-Cre* mice had fewer osteoclasts per bone area, as well as significantly decreased expression of the osteoclast-related gene *Rank*. Examination of NCM-derived factors that may be influencing osteoclastogenesis and bone resorption, such as *Rankl*, *Opg*, and *M-csf*, revealed no meaningful difference between *Tgfbr1*$^{fl/fl}$;*Wnt1-Cre* mice and controls, which suggests other NCM-derived factors are mediating the change in osteoclast number and osteoclast perimeter in *Tgfbr1*$^{fl/fl}$;*Wnt1-Cre* mice. Importantly, our premise that Tgfbr1 signaling is

10.3389/fphys.2024.1435594

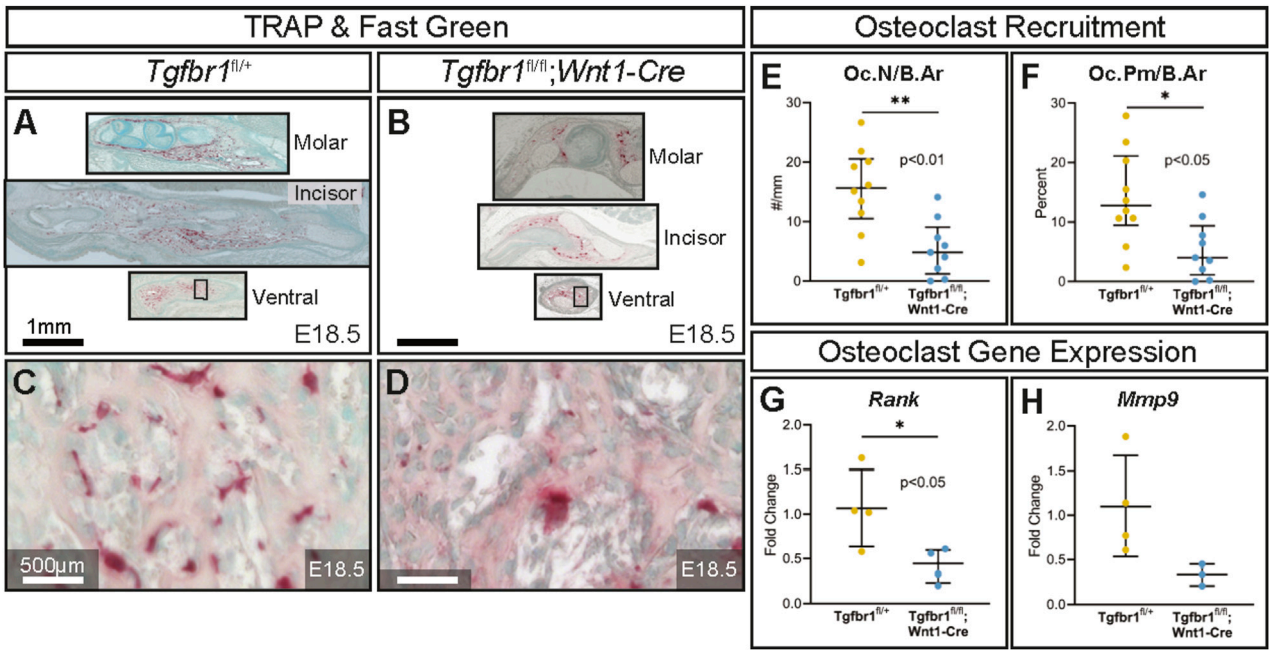


FIGURE 3
TGF-β signaling in the neural crest controls the amount of mandibular bone resorption. Adjacent transverse sections from mandibles that stained with Masson's trichrome were also stained with TRAP, which stains bone resorption red and methyl green from **(A)** control and **(B)** *Tgfbr1*$^{fl/fl}$*;Wnt1-Cre* E18.5 littermate embryos. Sections were stained and analyzed from three different regions in the mandible: molar, incisor, and ventral. Zoomed-in views from TRAP- and methyl green-stained ventral sections (black boxes) are shown for the **(C)** control and **(D)** *Tgfbr1*$^{fl/fl}$*;Wnt1-Cre* littermate E18.5 embryos. The sections were analyzed to determine whether there were differences in the amount of bone resorption. There were significant differences in bone resorption, as analyzed by **(E)** osteoclast number per bone area (Oc.N/B.Ar) and **(F)** osteoclast perimeter per bone area (Oc.Pm/B.Ar), with an approximately 3.2-fold decrease for both in the *Tgfbr1*$^{fl/fl}$*;Wnt1-Cre* mice when compared to control. **(G)** Using RT-qPCR to assay for *Rank* mRNA as a marker for the number of osteoclasts shows a significant 2.5-fold decrease in *Tgfbr1*$^{fl/fl}$*;Wnt1-Cre* at E18.5 when compared to controls. **(H)** Levels of *Mmp9* mRNA shows a 0.64-fold decrease in *Tgfbr1*$^{fl/fl}$*;Wnt1-Cre* at E18.5 when compared to controls.

inhibited in NCM-derived osteoblast lineage cells but intact in mesoderm-derived osteoclasts is supported by the fact that the bone phenotype of our embryonic *Tgfbr1*$^{fl/fl}$*;Wnt1-Cre* mice does not match the bone phenotype of mice with altered *Tgfbr2* in both osteoclasts and osteoblast lineage cells (Weivoda et al., 2016; Chai et al., 2023), and it is supported by the existing literature, which indicates there is no *Wnt1-Cre* signal in osteoclasts in calvarial bone (Laine et al., 2013).

It was previously established that *Tgfbr1*$^{fl/fl}$*;Wnt1-Cre* mandibles completely lack coronoid, condylar, and angular processes and are drastically smaller than control mandibles due to apoptosis between E10 and E14.5 in the proximal and aboral regions of the mandible (Dudas et al., 2006; Zhao et al., 2008). Our data suggest that the decrease in osteoclast number and osteoclast perimeter per bone area in *Tgfbr1*$^{fl/fl}$*;Wnt1-Cre* mandibles detected at E18.5 might be the mandibular bone trying to maintain bone quality and density following the previous apoptosis at E10–E14.5. We noted that bone volume was significantly lower in *Tgfbr1*$^{fl/fl}$*;Wnt1-Cre* mandibles at both E16.5 and E18.5, yet *Tgfbr1*$^{fl/fl}$*;Wnt1-Cre* mandible bone volume increased twice as much between these two stages as controls. This supports the hypothesis that the decrease in osteoclasts in *Tgfbr1*$^{fl/fl}$*;Wnt1-Cre* mandibles may occur to prevent additional bone loss following the E10–E14.5 apoptosis. Interestingly, although NCM-derived osteoblast lineage cells are known to regulate osteoclastogenesis, the lack of change in *Rankl*, *Opg*, *M-csf*, and *Rankl:Opg* in *Tgfbr1*$^{fl/fl}$*;Wnt1-Cre* mandibles suggests that these cells may regulate osteoclastogenesis through mechanisms other than modulating these factors. Wang et al. similarly found no change in the expression of *Rankl* or *Opg* in *Tgfbr2*$^{fl/fl}$*;Osx-Cre* alveolar bone despite a decrease in the osteoclast number and a decrease in TRAP-indicated bone resorption in the alveolar bone (Wang et al., 2013). Furthermore, the fact that *Tgfbr1*$^{fl/fl}$*;Wnt1-Cre* mandibles have bone quality similar to control mandibles suggests that the apoptosis noted by Dudas et al. and Zhao et al. may occur directly in the population of NCM destined to form the processes and part of the ramus portions of the developing mandible while not affecting the morphogenic units from the alveolar and body of the mandible (Atchley and Hall, 1991; Ehrich et al., 2003; Klingenberg et al., 2003; Dudas et al., 2006; Zhao et al., 2008). Further research is required to explore the possibility that NCM-derived osteoblast lineage cells influence osteoclast differentiation and activity to compensate for apoptosis in the proximal and aboral regions of *Tgfbr1*$^{fl/fl}$*;Wnt1-Cre* mandibles between stages E10 and E14.5.

We observed no difference in mandibular tissue mineral density in *Tgfbr1*$^{fl/fl}$*;Wnt1-Cre* embryos despite a decrease in osteoclast number, osteoclast perimeter per bone area, and *Rank* expression, which also merits further investigation into the mechanism through which osteoclast-deficient mandibles have tissue mineral density similar to that of controls. Additionally, unbiased techniques such as mRNA sequencing may indicate which factors are utilized by osteoblast lineage cells to influence osteoclasts at and before E18.5, the stage at which we observed a decrease in osteoclast number and perimeter. Future work will also seek to determine what aspect of osteoclastogenesis is

10.3389/fphys.2024.1435594

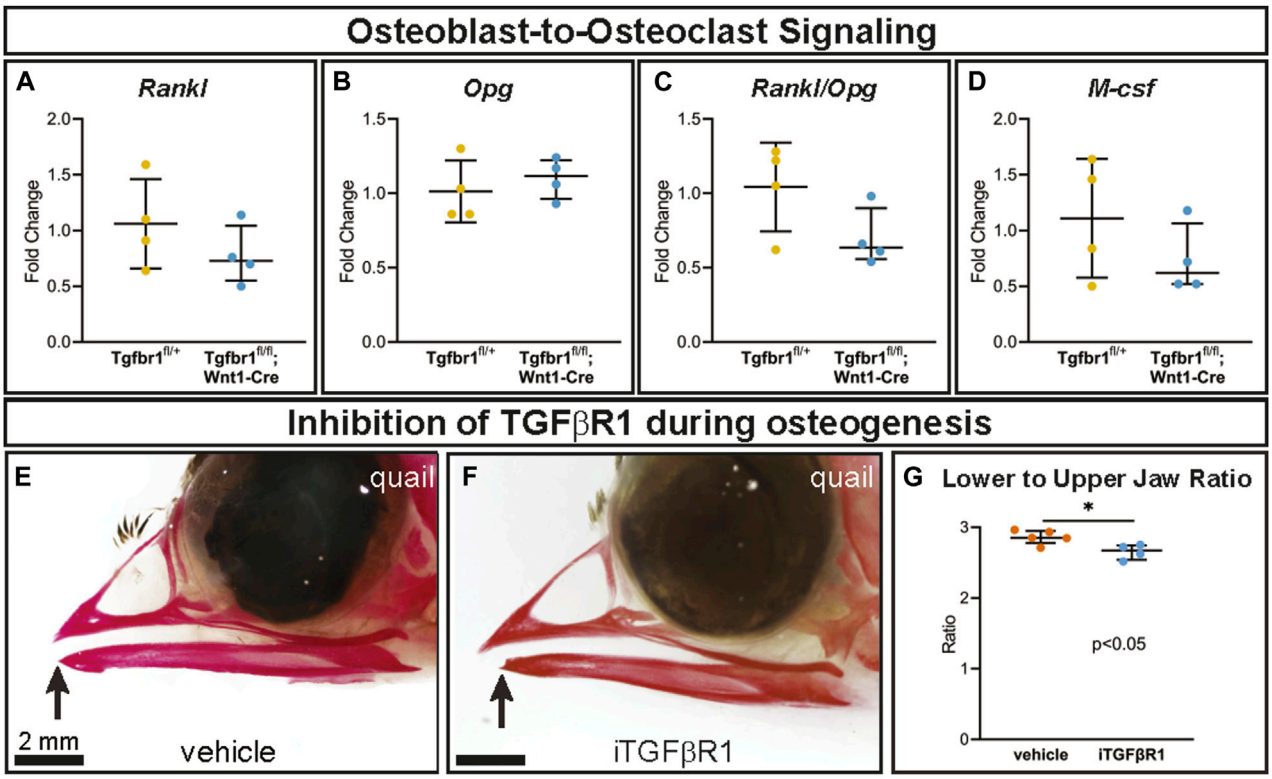


FIGURE 4
TGF-β signaling in the neural crest does not alter osteoblast-to-osteoclast signaling pathways through *Rankl*, *Opg*, or *M-csf*. Well-known signaling factors from the osteoblast lineage to osteoclasts are Rankl, Opg, and M-csf. Using RT-qPCR to assay for **(A)** *Rankl*, **(B)** *Opg*, **(C)** *Rankl/Opg*, and **(D)** *M-csf* mRNA expression revealed no significant difference in *Tgfbr1*$^{fl/fl}$;*Wnt1-Cre* at E18.5 compared to controls. To inhibit TGFBR1 after the apoptosis in *Tgfbr1*$^{fl/fl}$;*Wnt1-Cre* mice from E10–E14.5, we injected a TGFBR1 inhibitor (SB431542) into quail embryos at HH33, which by Carnegie staging is similar to an E15 mouse and therefore after the E10–E14.5 apoptosis. Embryos were collected at HH38 and stained with alizarin red, which stains calcified bone red. **(E)** In the vehicle-treated control quail, the upper and lower jaws align, but in the **(F)** TGFBR1 inhibitor-injected quail, the lower jaw is significantly shorter than the upper jaw. **(G)** The ratio of lower-to-upper jaw length is significantly less in the TGFBR1 inhibitor injected quail compared to the control-injected quail.

dysregulated in *Tgfbr1*$^{fl/fl}$;*Wnt1-Cre* mandibles. We saw a reduction in the osteoclast number and osteoclast perimeter per bone area, which may suggest that osteoclast proliferation was affected in *Tgfbr1*$^{fl/fl}$;*Wnt1-Cre* mandibles. However, our data indicated there was no change in the expression of *Rankl*, *Opg*, *Rankl/Opg*, or *M-csf* in *Tgfbr1*$^{fl/fl}$;*Wnt1-Cre* mandibles, suggesting osteoclast differentiation mediated by these factors should not have been affected. It has not yet been determined whether fusion or maturation of osteoclasts are affected in *Tgfbr1*$^{fl/fl}$;*Wnt1-Cre* mandibles.

It has previously been shown that inhibition of osteocyte TGF-β signaling in postnatal long bone dysregulates osteocytic osteolysis (Mohammad et al., 2009; Dole et al., 2017). Pharmacologic inhibition of Tgfbr1 between P35 and P77 impairs perilacunar/canalicular remodeling in long bone, and loss of *Tgfbr2* in osteocytes resulted in a decrease in trabecular separation, increase in trabecular number, decrease in *Rankl/Opg* ratio, and decrease in *Mmp13* expression in long bone. None of these values differed between controls and *Tgfbr1*$^{fl/fl}$;*Wnt1-Cre* embryos in our data, which suggests that perilacunar/canalicular remodeling is not the mechanism responsible for the large decrease in gross mandibular size and mandibular bone volume seen in *Tgfbr1*$^{fl/fl}$;*Wnt1-Cre* embryos. It is possible that the loss of Tgfbr1 in osteocytes prevented some perilacunar/canalicular remodeling in *Tgfbr1*$^{fl/fl}$;*Wnt1-Cre* embryo mandibles; however, perilacunar/canalicular remodeling during mandibular embryonic development has yet to be explored.

Embryonic quail given a single dose of iTGFBR1, specifically at the developmental timepoint when the lower jaw is just beginning to mineralize and just prior to osteoclast bone resorption beginning in the lower jaw, had a short lower jaw. This demonstrates that inhibition of typical TGFBR1 activity results in a shorter lower jaw despite the drug being delivered *after* the timepoint at which apoptosis was seen in the *Tgfbr1*$^{fl/fl}$;*Wnt1-Cre* mandibles at E10–E14.5. Utilizing an inducible cre mouse model to excise *Tgfbr1* after E14.5 could reveal the role of NCM-controlled osteoclastogenesis and bone resorption in mandible development, independent of the apoptosis seen in the proximal and aboral regions of *Tgfbr1*$^{fl/fl}$;*Wnt1-Cre* mandibles at E10–E14.5 in a mammalian model. Such a model would provide more insight into whether TGF-β signaling in NCM is a critical pathway by which osteocytes influence osteoclast activity and jaw length. It would also clarify at which timepoints TGF-β signaling meaningfully influences jaw development and length.

In summary, osteoclasts have historically not been considered an important cell type in embryonic bone development but rather a cell type that is primarily involved in maintaining mature and aging bone. However, emerging evidence demonstrates that osteoclasts are critical for proper embryonic mandibular bone development (Ealba

et al., 2015; Hassan et al., 2023; Houchen et al., 2023). To explore the relationship between NCM-derived osteoblast lineage cells and mesoderm-derived osteoclasts during embryonic mandibular development, our experiment recapitulated the mandibular defects previously described in *Tgfbr1*$^{fl/fl}$*;Wnt1-Cre* mice and explored the status of osteoclasts in the mandibles of *Tgfbr1*$^{fl/fl}$*; Wnt1-Cre* mice. Though a decrease in the osteoclast number, osteoclast perimeter, and *Rank* and *Mmp9* expression were detected in *Tgfbr1*$^{fl/fl}$*;Wnt1-Cre* mandibles, NCM-derived osteoblast lineage signaling to osteoclasts was not indicated by a change in *Rankl*, *Opg*, or *M-csf* expression. The micrognathia phenotype of the *Tgfbr1*$^{fl/fl}$*;Wnt1-Cre* embryos was established following the apoptosis in the proximal and aboral regions of the mandible between E10 and E14.5 prior to initial osteoclast formation in the developing mandible at E14.5, and we hypothesize that the reduction in osteoclasts seen at E18.5 is protective of the bone volume in the *Tgfbr1*$^{fl/fl}$*;Wnt1-Cre* micrognathic jaw. The results of this study support the idea that there is a crosstalk between osteoblast lineage cells and osteoclasts during embryonic development as well as in mature bone and during aging. Further investigation would elucidate the mechanism by which NCM-derived osteoblast lineage cells influence osteoclasts during mandibular development when TGFBR1 signaling is altered. In addition, further investigation of TGFBR1 signaling will improve our understanding of Loeys–Dietz Syndrome I and our ability to treat patients with the syndrome. Growing evidence points toward osteoclasts having a role in the determination of jaw bone length under the direction of NCM-derived osteoblast lineage cells, making additional research into the mechanisms by which this relationship occurs critical for understanding mandibular development and, in turn, for developing therapies for all individuals with mandibular malformations.

## Data availability statement

The raw data supporting the conclusions of this article will be made available by the authors, without undue reservation.

## Ethics statement

The animal study was approved by Institutional Animal Care and Use Committee at the University of Michigan. The study was conducted in accordance with the local legislation and institutional requirements.

## Author contributions

CH: data curation, formal analysis, investigation, visualization, writing–original draft, and writing–review and editing. SG: data curation, formal analysis, investigation, methodology, visualization, writing–original draft, and writing–review and editing. VK: conceptualization, investigation, project administration, resources, supervision, writing–original draft, and writing–review and editing. EB: conceptualization, data curation, formal analysis, funding acquisition, investigation, methodology, project administration, resources, supervision, visualization, writing–original draft, and writing–review and editing.

## Funding

The author(s) declare that financial support was received for the research, authorship, and/or publication of this article, funded in part by the University of Michigan Undergraduate Research Opportunity Program Biomedical and Life Sciences Sumer Research Opportunity Program to SG, NIDCR R01 DE13085 to VK, NICDR K08 DE021705 to EB, and NIH/NCRR S10RR026475-01 to the University of Michigan School of Dentistry Micro-CT core.

## Acknowledgments

The authors thank J. Lane, S. Rajderkar, and P. Thomas for suggestions and technical support, B. Pierchala for use and technical support of the Zeiss Microscope and AxioVision software, C. Merceron and E. Schipani for use and technical support of BioQuant Osteo software, B. Allen for use of egg incubators and micro-injector, M. Lynch in the University of Michigan School of Dentistry Micro-CT Core for scans, C. Strayhorn in the Histology Core for Masson's trichrome staining, and D. Folk and S. Hall for writing support through the BioKansas Scientific Writing Program. The original manuscript was previously submitted to bioRxiv.

## Conflict of interest

The authors declare that the research was conducted in the absence of any commercial or financial relationships that could be construed as a potential conflict of interest.

The author(s) declared that they were an editorial board member of Frontiers, at the time of submission. This had no impact on the peer review process and the final decision.

## Publisher's note

# References


Ainsworth, S. J., Stanley, R. L., and Evans, D. J. (2010). Developmental stages of the Japanese quail. *J. Anat.* 216 (1), 3–15. doi:10.1111/j.1469-7580.2009.01173.x

Albanese, C. T., and Harrison, M. R. (1998). Surgical treatment for fetal disease. The state of the art. *Ann. N. Y. Acad. Sci.* 847, 74–85. doi:10.1111/j.1749-6632.1998.tb08928.x

Alliston, T., Choy, L., Ducy, P., Karsenty, G., and Derynck, R. (2001). TGF-beta-induced repression of CBFA1 by Smad3 decreases cbfa1 and osteocalcin expression and inhibits osteoblast differentiation. *Embo J.* 20 (9), 2254–2272. doi:10.1093/emboj/20.9.2254

Atchley, W. R. (1993). Genetic and developmental aspects of variability in the mammalian mandible. *skull* 1, 207–247. doi:10.1086/419314

Atchley, W. R., and Hall, B. K. (1991). A model for development and evolution of complex morphological structures. *Biol. Rev. Camb Philos. Soc.* 66 (2), 101–157. doi:10.1111/j.1469-185x.1991.tb01138.x

Attisano, L., and Wrana, J. L. (2002). Signal transduction by the TGF-beta superfamily. *Science* 296 (5573), 1646–1647. doi:10.1126/science.1071809

Barlow, A. J., and Francis-West, P. H. (1997). Ectopic application of recombinant BMP-2 and BMP-4 can change patterning of developing chick facial primordia. *Development* 124 (2), 391–398. doi:10.1242/dev.124.2.391

Bustin, S. A., Benes, V., Garson, J. A., Hellemans, J., Huggett, J., Kubista, M., et al. (2009). The MIQE guidelines: minimum information for publication of quantitative real-time PCR experiments. *Clin. Chem.* 55 (4), 611–622. doi:10.1373/clinchem.2008.112797

Cakan, D. G., Ulkur, F., and Taner, T. U. (2012). The genetic basis of facial skeletal characteristics and its relation with orthodontics. *Eur. J. Dent.* 6 (3), 340–345. doi:10.1055/s-0039-1698971

Chai, W., Hao, W., Liu, J., Han, Z., Chang, S., Cheng, L., et al. (2023). Visualizing cathepsin K cre expression at the single cell level with GFP reporters. *J. Bone Mineral Res. Plus* 7 (1), e10706. doi:10.1002/jbm4.10706

Danielian, P. S., Muccino, D., Rowitch, D. H., Michael, S. K., and McMahon, A. P. (1998). Modification of gene activity in mouse embryos *in utero* by a tamoxifen-inducible form of Cre recombinase. *Curr. Biol.* 8 (24), 1323–1326. doi:10.1016/s0960-9822(07)00562-3

Dempster, D. W., Compston, J. E., Drezner, M. K., Glorieux, F. H., Kanis, J. A., Malluche, H., et al. (2013). Standardized nomenclature, symbols, and units for bone histomorphometry: a 2012 update of the report of the ASBMR Histomorphometry Nomenclature Committee. *J. Bone Min. Res.* 28 (1), 2–17. doi:10.1002/jbmr.1805

Derynck, R., and Zhang, Y. E. (2003). Smad-dependent and Smad-independent pathways in TGF-beta family signalling. *Nature* 425 (6958), 577–584. doi:10.1038/nature02006

Dole, N. S., Mazur, C. M., Acevedo, C., Lopez, J. P., Monteiro, D. A., Fowler, T. W., et al. (2017). Osteocyte-intrinsic TGF-β signaling regulates bone quality through perilacunar/canalicular remodeling. *Cell. Rep.* 21 (9), 2585–2596. doi:10.1016/j.celrep.2017.10.115

Dudas, M., Kim, J., Li, W. Y., Nagy, A., Larsson, J., Karlsson, S., et al. (2006). Epithelial and ectomesenchymal role of the type I TGF-beta receptor ALK5 during facial morphogenesis and palatal fusion. *Dev. Biol.* 296 (2), 298–314. doi:10.1016/j.ydbio.2006.05.030

Ealba, E. L., Jheon, A. H., Hall, J., Curantz, C., Butcher, K. D., and Schneider, R. A. (2015). Neural crest-mediated bone resorption is a determinant of species-specific jaw length. *Dev. Biol.* 408, 151–163. doi:10.1016/j.ydbio.2015.10.001

Ehrich, T. H., Vaughn, T. T., Koreishi, S. F., Linsey, R. B., Pletscher, L. S., and Cheverud, J. M. (2003). Pleiotropic effects on mandibular morphology I. Developmental morphological integration and differential dominance. *J. Exp. Zool. B Mol. Dev. Evol.* 296 (1), 58–79. doi:10.1002/jez.b.9

Gorlin, R. J., Cohen, M. M., and Levin, L. S. (1990). *Syndromes of the head and neck*. China: Oxford University Press.

Hall, J., Jheon, A. H., Ealba, E. L., Eames, B. F., Butcher, K. D., Mak, S.-S., et al. (2014). Evolution of a developmental mechanism: species-specific regulation of the cell cycle and the timing of events during craniofacial osteogenesis. *Dev. Biol.* 385 (2), 380–395. doi:10.1016/j.ydbio.2013.11.011

Hamburger, V., and Hamilton, H. L. (1951). A series of normal stages in the development of the chick embryo. *J. Morphol.* 88 (1), 49–92. doi:10.1002/jmor.1050880104

Hassan, M. G., Vargas, R., Zhang, B., Marcel, N., Cox, T. C., and Jheon, A. H. (2023). Altering osteoclast numbers using CTSK models *in utero* affects mice offspring craniofacial morphology. *Orthod. Craniofacial Res.* 26 (3), 338–348. doi:10.1111/ocr.12614

Houchen, C. J., Castro, B., Hahn Leat, P., Mohammad, N., Hall-Glenn, F., and Bumann, E. E. (2023). Treatment with an inhibitor of matrix metalloproteinase 9 or cathepsin K lengthens embryonic lower jaw bone. *Orthod. Craniofacial Res.* 26, 500–509. doi:10.1111/ocr.12635

Kaufman, M. H. (1992). *The altas of mouse development*, 59. No Title).

Klingenberg, C. P., Mebus, K., and Auffray, J. C. (2003). Developmental integration in a complex morphological structure: how distinct are the modules in the mouse mandible? *Evol. Dev.* 5 (5), 522–531. doi:10.1046/j.1525-142x.2003.03057.x

Lacombe, D., and Battin, J. (1993). Marfanoid features and craniosynostosis: report of one case and review. *Clin. Dysmorphol.* 2 (3), 220–224. doi:10.1097/00019605-199307000-00005

Laine, C. M., Joeng, K. S., Campeau, P. M., Kiviranta, R., Tarkkonen, K., Grover, M., et al. (2013). WNT1 mutations in early-onset osteoporosis and osteogenesis imperfecta. *N. Engl. J. Med.* 368 (19), 1809–1816. doi:10.1056/NEJMoa1215458

Larsson, J., Goumans, M. J., Sjöstrand, L. J., Van Rooijen, M. A., Ward, D., Levéen, P., et al. (2001). Abnormal angiogenesis but intact hematopoietic potential in TGF-beta type I receptor-deficient mice. *EMBO J.* 20, 1663–1673. doi:10.1093/emboj/20.7.1663

Livak, K. J., and Schmittgen, T. D. (2001). Analysis of relative gene expression data using real-time quantitative PCR and the 2(-Delta Delta C(T)) Method. *Methods* 25 (4), 402–408. doi:10.1006/meth.2001.1262

Loeys, B. L., Chen, J., Neptune, E. R., Judge, D. P., Podowski, M., Holm, T., et al. (2005). A syndrome of altered cardiovascular, craniofacial, neurocognitive and skeletal development caused by mutations in TGFBR1 or TGFBR2. *Nat. Genet.* 37 (3), 275–281. doi:10.1038/ng1511

MacCarrick, G., Black, J. H., Bowdin, S., El-Hamamsy, I., Frischmeyer-Guerrerio, P. A., Guerrerio, A. L., et al. (2014). Loeys–Dietz syndrome: a primer for diagnosis and management. *Genet. Med.* 16 (8), 576–587. doi:10.1038/gim.2014.11

Malik, Z., Roth, D. M., Eaton, F., Theodor, J. M., and Graf, D. (2020). Mesenchymal Bmp7 controls onset of tooth mineralization: a novel way to regulate molar cusp shape. *Front. Physiology* 11, 698. doi:10.3389/fphys.2020.00698

Massague, J., and Wotton, D. (2000). Transcriptional control by the TGF-beta/Smad signaling system. *Embo J.* 19 (8), 1745–1754. doi:10.1093/emboj/19.8.1745

Mohammad, K. S., Chen, C. G., Balooch, G., Stebbins, E., McKenna, C. R., Davis, H., et al. (2009). Pharmacologic inhibition of the TGF-beta type I receptor kinase has anabolic and anti-catabolic effects on bone. *PloS one* 4 (4), e5275. doi:10.1371/journal.pone.0005275

Nagy, A. *Manipulating the mouse embryo: a laboratory manual*. Cold Spring Harbor, New.York.: Cold Spring Harbor Laboratory Press; 2003. x, 764 p. p.

Nakashima, T., Hayashi, M., Fukunaga, T., Kurata, K., Oh-Hora, M., Feng, J. Q., et al. (2011). Evidence for osteocyte regulation of bone homeostasis through RANKL expression. *Nat. Med.* 17 (10), 1231–1234. doi:10.1038/nm.2452

Oka, K., Oka, S., Sasaki, T., Ito, Y., Bringas, Jr P., Nonaka, K., et al. (2007). The role of TGF-beta signaling in regulating chondrogenesis and osteogenesis during mandibular development. *Dev. Biol.* 303 (1), 391–404. doi:10.1016/j.ydbio.2006.11.025

Peters, S. B., Wang, Y., and Serra, R. (2017). Tgfbr2 is required in osterix expressing cells for postnatal skeletal development. *Bone* 97, 54–64. doi:10.1016/j.bone.2016.12.017

Prasad, M. S., Charney, R. M., and García-Castro, M. I. (2019). Specification and formation of the neural crest: perspectives on lineage segregation. *Genesis* 57 (1), e23276. doi:10.1002/dvg.23276

Roth, D. M., Bayona, F., Baddam, P., and Graf, D. (2021). Craniofacial development: neural crest in molecular embryology. *Head Neck Pathology* 15 (1), 1–15. doi:10.1007/s12105-021-01301-z

S. L. Leary, W. Underwood, R. Anthony, S. Cartner, D. Corey, T. Grandin, et al. (2022). *AVMA guidelines for the euthanasia of animals: 2013 edition2013: American Veterinary Medical Association Schaumburg, IL* (USA: AVMA).

Schneider, C. A., Rasband, W. S., and Eliceiri, K. W. (2012). NIH Image to ImageJ: 25 years of image analysis. *Nat. methods* 9 (7), 671–675. doi:10.1038/nmeth.2089

Tang, S. Y., Herber, R. P., Ho, S. P., and Alliston, T. (2012). Matrix metalloproteinase–13 is required for osteocytic perilacunar remodeling and maintains bone fracture resistance. *J. Bone Mineral Res.* 27 (9), 1936–1950. doi:10.1002/jbmr.1646

Tatsumi, S., Ishii, K., Amizuka, N., Li, M., Kobayashi, T., Kohno, K., et al. (2007). Targeted ablation of osteocytes induces osteoporosis with defective mechanotransduction. *Cell. metab.* 5 (6), 464–475. doi:10.1016/j.cmet.2007.05.001

Theiler, K. (2013). *The house mouse: atlas of embryonic development*. Germany: Springer Science and Business Media.

Wang, Y., Cox, M. K., Coricor, G., MacDougall, M., and Serra, R. (2013). Inactivation of Tgfbr2 in Osterix-Cre expressing dental mesenchyme disrupts molar root formation. *Dev. Biol.* 382 (1), 27–37. doi:10.1016/j.ydbio.2013.08.003

Weivoda, M. M., Ruan, M., Pederson, L., Hachfeld, C., Davey, R. A., Zajac, J. D., et al. (2016). Osteoclast TGF-β receptor signaling induces Wnt1 secretion and couples bone resorption to bone formation. *J. Bone Mineral Res.* 31 (1), 76–85. doi:10.1002/jbmr.2586

Xiong, J., Piemontese, M., Onal, M., Campbell, J., Goellner, J. J., Dusevich, V., et al. (2015). Osteocytes, not osteoblasts or lining cells, are the main source of the RANKL required for osteoclast formation in remodeling bone. *PloS one* 10 (9), e0138189. doi:10.1371/journal.pone.0138189

Yuan, Y., Loh, Y.-hE., Han, X., Feng, J., Ho, T.-V., He, J., et al. (2020). Spatiotemporal cellular movement and fate decisions during first pharyngeal arch morphogenesis. *Sci. Adv.* 6 (51), eabb0119. doi:10.1126/sciadv.abb0119

Zhao, H., Oka, K., Bringas, P., Kaartinen, V., and Chai, Y. (2008). TGF-beta type I receptor Alk5 regulates tooth initiation and mandible patterning in a type II receptor-independent manner. *Dev. Biol.* 320 (1), 19–29. doi:10.1016/j.ydbio.2008.03.045